Measurement of Spin-Exchange Cross Sections for Cs^{133}, Rb^{87}, Rb^{85}, K^{39}, and Na^{23}†*

N. W. Ressler‡
Ford Scientific Laboratory, Dearborn, Michigan 48121
and
R. H. Sands
University of Michigan, Ann Arbor, Michigan 48104
and
T. E. Stark
University of California, Irvine, California 94538
(Received 1 April 1969)

This paper reports measurements to determine the spin-exchange cross section for collisions between like alkali atoms. The spin-exchange cross section is determined for Cs^{133}, Rb^{87}, Rb^{85}, K^{39}, and Na^{23}. The lifetime of the alkali atoms in the Zeeman sublevels of the ground-state hyperfine levels is dominated by spin-exchange collisions. The spin-exchange collision rate is therefore reflected by the linewidth of the microwave absorption spectrum observed in the magnetic dipole transitions between various of the Zeeman sublevels. The measurements employed an X-band electron paramagnetic resonance spectrometer. The alkali metal was distilled into a sample bulb which was placed inside a Dewar in a resonant cavity. The bulb was then heated to a temperature corresponding to an equilibrium vapor density of approximately 10^{15} alkali atoms/c.c. and the microwave absorption spectrum was recorded. In order to relate the spin-exchange rate to a cross section, it is necessary to determine the alkali density. This was done by comparing the intensity of the alkali EPR absorption to that of a weighed and oriented copper sulfate crystal. For Cs^{133} and Rb^{87}, interpretation of the linewidth data is complicated by the fact that the transitions occur in a region where there is appreciable mixing of the high-field spin states by the hyperfine interaction. A density-matrix description of spin exchange which corrects for this intermediate field mixing is discussed, and the corrections are applied to the measured cross sections for two transitions in Cs^{133} and Rb^{87}. Relative cross sections, referred to that of Na^{23}, are also given.

I. INTRODUCTION

This paper reports a measurement of the self-spin-exchange cross section for Cs^{133}, Rb^{87}, Rb^{85}, K^{39}, and Na^{23} at vapor densities between 10^{15} and 10^{16} atoms/c.c.

Interest in spin exchange began with Purcell and Field[1] who were interested in determining the effect of spin exchange upon the relative hyperfine populations of interstellar atomic hydrogen. At about the same time Wittke and Dicke[2] found that spin exchange was the dominant line-broadening mechanism in a precision measurement of the ground-state hyperfine splitting of atomic hydrogen.

Since that time spin exchange has been used to transfer spin polarization from one atomic species to another[3] and has been shown to be responsible for a small shift in the resonance frequency of the hydrogen, rubidium, and cesium maser.[4–6]

There have been numerous measurements[7] of the spin-exchange cross sections for cesium and rubidium. Most of these have utilized the techniques of optical pumping, for which determination of the alkali density (which is necessary in order to relate the relaxation rate to a cross section) is difficult.

The measurements reported here were made with an X-band electron paramagnetic resonance spectrometer.[8] The atomic transitions studied were between magnetic substates of the ground-state hyperfine states of the alkalis. Figure 1 shows the level structure of such states for an atom having nuclear spin $I = \frac{3}{2}$. This particular diagram describes Rb^{87}, and the two $\Delta M_F = +1$ transitions which were studied in Rb^{87} are indicated.

The width of the magnetic dipole absorption spectrum allows determination of the mean time

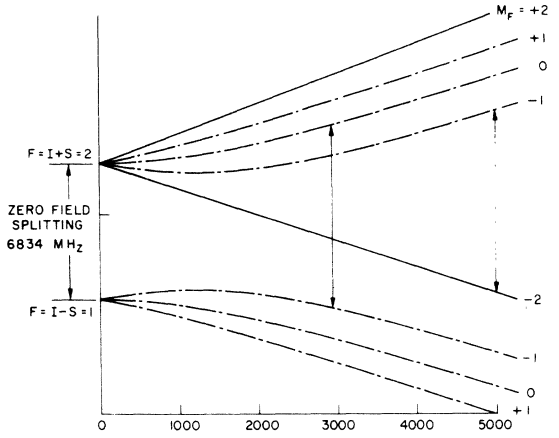

FIG. 1. Ground-state hyperfine magnetic sublevels for an alkali having nuclear spin $\frac{3}{2}$, as a function of the field in Gauss.

between spin-exchange collisions. The spin-exchange rate $(T_x)^{-1}$ is related to the spin-exchange cross section by the standard result from kinetic theory.

$$1/T_x = N\sigma_x\langle V_{\mathrm{rel}}\rangle ,$$

where N is the number density, σ_x is the spin-exchange cross section, and $\langle V_{\mathrm{rel}}\rangle$ is the mean relative velocity.

The alkali vapor density was determined by comparing the intensity of the alkali absorption spectrum to that of a weighed and oriented copper sulfate crystal.

A theoretical description of the effect of spin exchange upon the observables in the alkalis is given in Sec. II.

II. THEORETICAL DESCRIPTION OF SPIN EXCHANGE

In this section we examine the dynamical basis for spin exchange, and explore in some detail the role of exchange collisions in determining the lifetime of an electron in a given spin state.[9] Because the details of the motion of the atomic spins are of primary interest, attention may be confined to the spin system, taking into account its statistical character by means of the density-matrix formalism. It will be sufficient to regard the atoms themselves as being in definite but unspecified states of relative momentum before and after the collision. Furthermore, insofar as it is improbable that successive collisions would involve the same pair of atoms, the atoms may be regarded as statistically independent and hence uncorrelated.

Consider, then, two alkali atoms chosen at random from an assembly of N such atoms, and presumed about to collide. These atoms will interact through a spin-dependent central potential $V_S(r)$, where r is the distance between atoms, and S is the quantum number for the total electronic spin. Let $\Psi(1, 2)$ be the total wave function describing the pair of atoms preceding the collision and let $\Psi_C(1, 2)$ describe the atoms following the collision. It can be shown[10] that these wave functions are related by

$$\Psi_c(1, 2) = [F_d(\theta) + F_x(\theta)\vec{\sigma}_1 \cdot \vec{\sigma}_2]\Psi(1, 2) . \tag{1}$$

The amplitudes $F_d(\theta)$ and $F_x(\theta)$ are called the direct and exchange amplitudes, respectively. The total cross section for spin exchange is given by

$$Q_x = 2\pi \int |F_x(\theta)|^2 d(\cos\theta). \tag{2}$$

For the purposes of this paper it will be convenient to work with the partial amplitudes for direct and exchange scattering. These are defined by

$$F_d(\theta) = \frac{1}{k}\sum_{l=0}^{\infty} (2l+1) f_d^{(l)} P_l(\cos\theta) , \quad F_x(\theta) = \frac{1}{k}\sum_{l=0}^{\infty} (2l+1) f_x^{(l)} P_l(\cos\theta) . \tag{3}$$

Then[11] $$f_d^{(l)} = \tfrac{1}{4}(3e^{i\varphi_l(k)} + 1) , \quad f_x^{(l)} = \tfrac{1}{4}(e^{i\varphi_l(k)} - 1) , \tag{4}$$

and the total spin-exchange cross section is given by

$$Q_x = \frac{\pi}{k^2}\sum_{l=0}^{\infty} (2l+1)\sin^2\frac{\varphi_l(k)}{2} .$$

The phase shift $\varphi_l(k)$ arises from the very different boundary conditions imposed on the scattering process by the singlet potential $V_0(r)$ and the triplet potential $V_1(r)$. Depending on the values of the angular momentum l and relative kinetic energy $E = \hbar^2k^2/2\mu$, the phase shift is given by

$$\varphi_l(k) = \frac{1}{\hbar}\int_{-\infty}^{+\infty}[V_1(r) - V_0(r)]\,dt. \tag{5}$$

The operator $M_l(k) = f_d^{(l)} + f_x(l)\vec{\sigma}_1 \cdot \vec{\sigma}_2$ determines the effect of a single collision on the two-particle density matrix. With the assumption that the atoms are not correlated by previous encounters, the two-particle density matrix may be written as the direct product of single-particle density matrices

$$\rho(1,2) = \rho(1)\otimes\rho(2). \tag{6}$$

Following a collision the two-particle density matrix is given by

$$\rho_c(1,2) = M_l(k)\rho(1,2)M_l^*(k) \neq \rho_c(1)\otimes\rho_c(2)\ . \tag{7}$$

The density matrix for one of the atoms is recovered by taking the trace over $\rho_c(1,2)$ with respect to all quantities bearing the indices of the other atom. Using the definition of $M_l(k)$, it follows that

$$\begin{aligned}[\rho_c(1)]_{ij} = {} & \tfrac{1}{4}(4 - 3\sin^2\varphi/2)[\rho(1)]_{ij} + \tfrac{1}{4}\sin^2(\varphi/2)\sum_{\alpha=x,y,z}[\sigma_\alpha\rho(1)\sigma_\alpha]_{ij} \\ & + \tfrac{1}{16}(1 - e^{-i\varphi})(3 + e^{+i\varphi})\sum_{\alpha=x,y,z}[\sigma_\alpha\rho(1)]_{ij}T_{R(2)}[\sigma_\alpha\rho(2)] \\ & + \tfrac{1}{16}(1 - e^{+i\varphi})(3 + e^{-i\varphi})\sum_{\alpha=x,y,z}[\rho(1)\sigma_\alpha]_{ij}T_{R(2)}[\sigma_\alpha\rho(2)] \\ & - \frac{i}{4}\sin^2(\varphi/2)\sum_{\alpha=x,y,z}\{[\sigma_\alpha\rho(1)\sigma_\beta]_{ij} - [\sigma_\beta\rho(1)\sigma_\alpha]_{ij}\}T_{R(2)}[\sigma_\gamma\rho(2)]\ ,\end{aligned} \tag{8}$$

where the normalization $T_{R(1)}\rho(1) = T_{R(2)}\rho(2) = 1$ has been assumed and where, in the last term, $\alpha\beta\gamma$ form a cyclic permutation of x, y, z. For simplicity the labels on $\varphi_l(k)$ have been dropped.

In the absence of collisions, the single-particle density matrix is free to evolve in time according to the usual equation of motion

$$i\hbar\frac{\partial\rho}{\partial t} = [\mathcal{H}, \rho]\ , \tag{9}$$

where $\mathcal{H}$ is the (spin) Hamiltonian to be described below. A single collision has the effect of providing an initial condition to the solution of Eq. (9). If t_0 is the time of the *last* collision, the density matrix will at all later times depend at least parametrically on t_0. Following Karplus and Schwinger[12] an average density matrix can be defined as

$$\bar{\rho}(t) = \frac{1}{\tau_c}\int_{-\infty}^{t}\rho(t, t_0)e^{-(t,t_0)/\tau_c}\,dt_0\ , \tag{10}$$

where $(\tau_c)^{-1}$ is the mean collision rate. The *form* of the density matrix $\rho(t_0, t_0) \equiv \rho_c$ defines the type of collision that has occurred. Karplus and Schwinger show that the average density matrix evolves according to the equation of motion

$$\frac{\partial\bar{\rho}}{\partial t} = -\frac{i}{\hbar}[\mathcal{H}, \bar{\rho}] - \frac{1}{\tau_c}(\bar{\rho} - \rho_c)\ . \tag{11}$$

In the present problem, that of describing the evolution of the density matrix in the presence of exchange collisions, the mean collision rate is given by

$$\tau_c^{-1} = N\langle V_{\text{rel}}\rangle\ \frac{\pi}{k^2}\sum_{l=0}^{\infty}(2l+1)\sin^2\frac{\varphi_l(k)}{2}\ , \tag{12}$$

where N is the number of atoms per unit volume and $\langle V_{\mathrm{rel}}\rangle$ is mean relative velocity of the atoms. The density matrix ρ_c is given by Eq. (8).

Spin exchange does not provide a mechanism for restoring thermal equilibrium to a spin system. Energy added to the spin system by external fields cannot reappear at the walls of the container, but rather is distributed by exchange collisions in such a way as to equalize the populations of all the levels. Relaxation may be provided for by including in the equation of motion the additional term $-(1/T_1)(\bar{\rho}-\rho_0)$, where ρ_0 is the density matrix describing thermal equilibrium among the spin states at a temperature T. The mean relaxation rate is T_1^{-1}. Thus the equation of motion to be solved is

$$\frac{\partial\bar{\rho}}{\partial t} = -\frac{i}{\hbar}[\mathcal{H},\bar{\rho}] - \frac{i}{\hbar}[\mathcal{H},\rho] - \frac{1}{\tau_c}(\bar{\rho}-\rho_c) - \frac{1}{T_1}(\bar{\rho}-\rho_0)\ . \tag{13}$$

For a static magnetic field $\hat{z}\,H_0$ and a microwave frequency magnetic field $\hat{x}2H_1\cos\omega t$, the spin Hamiltonian for an alkali atom is

$$\mathcal{H} = g_S\mu_0 H_0 S_z + A\vec{\mathrm{I}}\cdot\vec{\mathrm{S}} + 2\mu_0 g_S H_1 S_x\cos\omega t = \mathcal{H}_0 + \mathcal{H}(t)\ , \tag{14}$$

where μ_0 is the Bohr magneton and A measures the Fermi contact interaction. Terms proportional to the nuclear g value have been deleted, since $g_I \approx g_S/2000$. Also $2H_1 \ll H_0$ so that $\mathcal{H}(H)$ may be treated as a perturbation. The eigenvalues of $\mathcal{H}_0$, for $S = \frac{1}{2}$ and arbitrary field strengths, are given by the well-known Breit-Rabi formula.[13] The corresponding eigenfunctions (normalized) are most conveniently written in the high-field or uncoupled representation and are given by

$$|F,M\rangle = |M_I = I, M_S = \tfrac{1}{2}\rangle, \quad \text{for } M = I+\tfrac{1}{2}; \qquad |F,M\rangle = |M_I = I, M_S = -\tfrac{1}{2}\rangle, \quad \text{for } M = -(I+\tfrac{1}{2})\ ;$$

$$\text{and} \quad |F,M\rangle = A_M|M_I = M-\tfrac{1}{2}, M_S = +\tfrac{1}{2}\rangle + B_M|M_I = M+\tfrac{1}{2}, M_S = -\tfrac{1}{2}\rangle\ ,$$
$$|F-1,M\rangle = -B_M|M_I = M-\tfrac{1}{2}, M_S = +\tfrac{1}{2}\rangle + A_M|M_I = M+\tfrac{1}{2}, M_S = -\tfrac{1}{2}\rangle, \quad M = (I-\tfrac{1}{2}), \ldots, -(I-\tfrac{1}{2})\ ; \tag{15a}$$

$$\text{where} \quad A_M = \lambda_M/(\lambda_M^2+\lambda_M^2)^{1/2}, \quad B_M = \Lambda_M/(\lambda_M^2+\lambda_M^2)^{1/2}, \quad \lambda_M = [2/(2I+1)][(I+M+\tfrac{1}{2})(I-M+\tfrac{1}{2})]^{1/2},$$
$$\Lambda_M = -X - 2M/(2I+1) + [1+4MX/(2I+1)+X^2]^{1/2}, \quad X = [2g_S/(2I+1)]\,\mu_0 H_0/A, \quad F = I+\tfrac{1}{2}\ . \tag{15b}$$

These energy eigenfunctions are used to construct the density matrix $\bar{\rho}$, the matrix being of dimension $2(2I+1)$. In this representation ρ_0 is a diagonal matrix, the diagonal elements being equal to the fractional population of the corresponding energy states.

The oscillating magnetic field will cause the appearance of certain off-diagonal matrix elements in $\bar{\rho}$. It can be shown that so long as the various possible transitions with $\mathcal{H}_0$ are well resolved, the only non-negligible off-diagonal matrix elements will correspond to those eigenstates of $\mathcal{H}_0$ that are (nearly) resonantly coupled by the microwave field.

III. HIGH-FIELD CASE

The general solution of the equation of motion for $\bar{\rho}$ is out of the question. However, an approximate solution for the case of any nuclear spin I and large static magnetic fields ($X \gtrsim 2$) is relatively straightforward. The case of $I = \frac{1}{2}$ (hydrogen) will serve to illustrate the nature of the approximations used throughout this section. For this so-called high-field case the basis states are, from Eqs. (15),

$$|1\rangle = |M_I = \tfrac{1}{2}, M_S = \tfrac{1}{2}\rangle, \quad |2\rangle = |M_I = -\tfrac{1}{2}, M_S = \tfrac{1}{2}\rangle, \quad |3\rangle = |M_I = \tfrac{1}{2}, M_S = -\tfrac{1}{2}\rangle, \quad |4\rangle = |M_I = -\tfrac{1}{2}, M_S = -\tfrac{1}{2}\rangle\ . \tag{16}$$

For the transition $|3\rangle \rightarrow |1\rangle$ the only off-diagonal matrix elements are ρ_{13} and $\rho_{31} = \rho_{13}^*$. The following

equations of motion for the average density matrix are obtained from the general Eqs. (8) and (13) in the limit where the system is described by the high-field basis states (for simplicity $\bar{\rho}$ is written as ρ).

$$\dot{\rho}_{11} = -i\omega_1(\rho_{31}-\rho_{13})\cos\omega t - T_x^{-1}[\tfrac{1}{2}(1-Z)\rho_{11} - \tfrac{1}{2}(1+Z)\rho_{33}] - T_1^{-1}(\rho_{11}-\rho_{11}^{0}) \tag{17a}$$

$$\dot{\rho}_{22} = -T_x^{-1}[\tfrac{1}{2}(1-Z)\rho_{22} - \tfrac{1}{2}(1+Z)\rho_{44}] - T_1^{-1}(\rho_{22}-\rho_{22}^{0}) \tag{17b}$$

$$\dot{\rho}_{33} = +i\omega_1(\rho_{31}-\rho_{13})\cos\omega t - T_x^{-1}[\tfrac{1}{2}(1+Z)\rho_{33} - \tfrac{1}{2}(1+Z)\rho_{11}] - T_1^{-1}(\rho_{33}-\rho_{33}^{0}) \tag{17c}$$

$$\dot{\rho}_{44} = -T_x^{-1}[\tfrac{1}{2}(1+Z)\rho_{44} - \tfrac{1}{2}(1-Z)\rho_{22}] - T_1^{-1}(\rho_{44}-\rho_{44}^{0}) \tag{17d}$$

$$\dot{\rho}_{13} = \rho_{31}^{*} = -i\omega_{13}\rho_{13} + i\omega_1(\rho_{11}-\rho_{33})\cos\omega t - T_x^{-1}[1-(\rho_{11}+\rho_{33})]\rho_{13} - T_1^{-1}\rho_{13} \,. \tag{17e}$$

In these equations $T_x^{-1} = \tau_x^{-1}\sin^2(\varphi/2)$ is the mean rate at which exchange collisions occur, $\omega_{13} = (1/\hbar)(E_1 - E_3)$, $\omega_1 = 2\gamma H_1$, where γ, the gyromagnetic ratio $= (2/\hbar)\langle 1|\mu_x|3\rangle$, and $Z = T_R(\sigma_z\rho) = (\rho_{11}+\rho_{22}) - (\rho_{33}+\rho_{44})$ is the polarization of the sample. In the equation for ρ_{13} a small term leading to an exchange-induced frequency shift has been dropped. Bender[4] has calculated this shift as it applied to the hydrogen maser.

Letting $z = \rho_{11}-\rho_{33}$, $x = T_R(\sigma_x\rho) = \rho_{13}+\rho_{31}$, $y = T_R(\sigma_y\rho) = i(\rho_{13}-\rho_{31})$, and $n = \rho_{11}+\rho_{33}$, one finds from Eqs. (17b) and (17d)

$$\frac{d}{dt}(Z-z) \equiv \dot{\rho}_{22} - \dot{\rho}_{44} = -\frac{1}{T_x}[(Z-z) - Z(1-n)] - \frac{1}{T_1}[(Z-z) - (Z-z)_0] \,,$$

$$\frac{d}{dt}(1-n) \equiv \dot{\rho}_{22} + \dot{\rho}_{44} = -\frac{1}{T_1}[(1-n) - (1-n)_0] \,. \tag{18}$$

In the high-temperature approximation ($kT \gg \mu H_0$), the equilibrium distribution of population is nearly uniform over the spin states; then $\rho_{22}^{0} \approx \rho_{44}^{0} \approx \frac{1}{4}$, $(1-n) \approx \frac{1}{2}$, and $Z_0 \approx 2z_0$, so that

$$(1-n) = (1-n)_0 \approx \tfrac{1}{2}, \quad (Z-z) \approx \left(\frac{1}{T_1} + \frac{1}{2T_x}\right)^{-1}\left(\frac{1}{T_1}z_0 + \frac{1}{2T_x}z\right) \,. \tag{19}$$

Using these results the remaining equations can be combined to give

$$\dot{z} = 2\omega_1 y\cos\omega t - \tau_1^{-1}(z-z_0), \quad \dot{x} = \omega_{13}y - \tau_2^{-1}x, \quad \dot{y} = +\omega_{13}x - 2\omega_1 z\cos\omega t - \tau_2^{-1}y \,, \tag{20}$$

where $\tau_2^{-1} = T_1^{-1} + \frac{1}{2}T_x^{-1}$, and $\tau_1^{-1} = T_1^{-1} + (T_1 + 2T_x)^{-1}$.

Equations (20) may be compared with the well-known Bloch equations: τ_2 is the effective spin-spin relaxation time responsible for the observed spectral linewidth, and τ_1 is the spin-lattice relaxation time governing the return of a disturbed spin system to thermal equilibrium. The solutions to the Bloch equations are part of the standard literature on magnetic resonance.[14] The components of the complex susceptibility are found to be

$$\chi'(\omega) = \tfrac{1}{2}\chi_0\tau_2\omega_{13}\tau_2(\omega_{13}-\omega)/[1+\tau_2^{2}(\omega_{13}-\omega)^2 + \gamma^2 H_1^{2}\tau_1\tau_2],$$

$$\chi''(\omega) = \tfrac{1}{2}\chi_0\tau_2\omega_{13}/[1+\tau_2^{2}(\omega_{13}-\omega)^2 + \gamma^2 H_1^{2}\tau_1\tau_2] \,, \tag{21}$$

where χ_0 is the static susceptibility and $\gamma = (2/\hbar)\langle 1|\mu_x|3\rangle$.
The power absorbed by the sample is

$$P(\omega) = \frac{\omega}{2\pi}\int_0^{\omega/2\pi} \vec{B}\cdot\frac{d\vec{M}}{dt} = 2\omega\chi''(\omega)H_1^{2} \,. \tag{22}$$

The preceding formalism generalizes directly to the (high-field) case $I > \frac{1}{2}$. The reason is that for all the alkalis $S = \frac{1}{2}$, so one can couple $\vec{S}$ to any $\vec{I}$ in only two ways. This means that the off-diagonal elements

of the Hamiltonian are grouped as 2×2 submatrices along the diagonal, each submatrix corresponding to a given value of $M=M_I+M_S$. With hydrogen the problem has been solved with one of these 2×2 submatrices. For the general case of arbitrary nuclear spin I, one finds $(1-n)_0\approx 1/2I+1$ and $Z_0\approx(2I+1)z_0$. The solutions carry through unchanged, except that the spin-spin and spin-lattice relaxation times have the general form given in Eq. (23), that is,

$$\frac{1}{\tau_2}=\frac{1}{T_1}+\frac{2I}{2I+1}\,\frac{1}{T_x}\,,\qquad \frac{1}{\tau_1}=\frac{1}{T_1}+\left(\frac{1}{2I}\,T_1+\frac{2I+1}{2I}\,T_x\right)^{-1}\,. \tag{23}$$

The general relaxation rates for the high-field case given by Eqs. (23) can be derived by considering an equivalent circuit of the relaxation mechanisms which are available to the spin system. Figure 2 gives such an equivalent circuit where it is assumed that microwave power is being supplied to one pair of magnetic sublevels. This pair of sublevels is coupled to the remaining $2I$ pairs of levels through spin exchange, and all pairs of levels are coupled to the "lattice" through an assumed spin-lattice relaxation mechanism characterized by a rate $(T_1)^{-1}$.

The theory developed so far is directly applicable to X-band microwave transitions in Rb^{85}, K^{39}, and Na^{23}. For sufficiently weak rf fields $(\gamma^2B_1^2\tau_1\tau_2\ll 1)$, the theory predicts a Lorentzian line shape with a full width at half-maximum given by τ_2^{-1}.

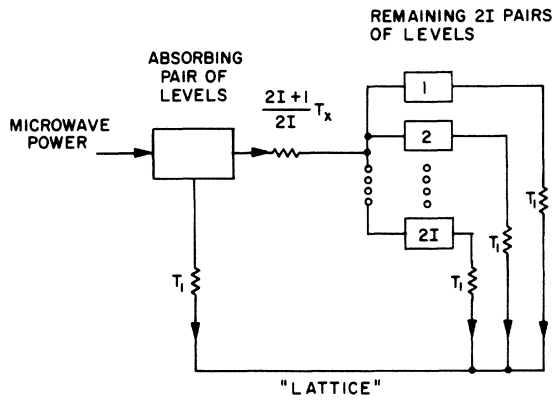

FIG. 2. Equivalent circuit of the relaxation mechanisms available to a spin system in steady state.

IV. INTERMEDIATE-FIELD CASE

The microwave transitions in Rb^{87} and Cs^{133} fall in the intermediate-field region $(X\lesssim 2)$. In this region there is the possibility that because the electron and nucleus are not decoupled, the "effective" collision rate for spin exchange between specified energy states is thereby affected. That is indeed the case.

A complete solution to the intermediate-field problem has not been obtained. However, it is possible to examine the density-matrix equations when there is no saturation $(\gamma^2B_1{}^2\tau_1\tau_2\ll 1, Z\approx Z_0)$ and to compute this correction.

The solution will again be illustrated with hydrogen. Information concerning the effect of the hyperfine coupling between the electron and nuclear spin upon the effective spin-spin relaxation rate is contained in the off-diagonal matrix elements of the density matrix.

The intermediate-field eigenstates for hydrogen in terms of the high-field basis states are given by Eqs. (15) for the case $M_S=M_I=\pm\frac{1}{2}$. These are written

$$\begin{aligned}
|1\rangle &= |M_I=+\tfrac{1}{2},\ M_S=+\tfrac{1}{2}\rangle,\\
|2\rangle &= A_0|M_I=-\tfrac{1}{2},\ M_S=+\tfrac{1}{2}\rangle+B_0|M_I=+\tfrac{1}{2},M_S=-\tfrac{1}{2}\rangle,\\
|3\rangle &= -B_0|M_I=-\tfrac{1}{2},\ M_S=+\tfrac{1}{2}\rangle+A_0|M_I=+\tfrac{1}{2},M_S=-\tfrac{1}{2}\rangle,\\
|4\rangle &= |M_I=-\tfrac{1}{2},\ M_S=-\tfrac{1}{2}\rangle\,.
\end{aligned} \tag{24}$$

It is straightforward but laborious computation to write out the relevant density-matrix elements from Eqs. (8) and (13) using the intermediate-field wave functions given by Eq. (16). Referring to Eq. (17e) it is seen that the term describing the spin-spin relaxation rate has the form[15]

$$\begin{aligned}
&[\sin^2(\varphi/2)/\tau_x][1-(\rho_{11}+\rho_{22})]\rho_{13}\\
&\quad=[\sin^2(\varphi/2)/\tau_x]\{\tfrac{1}{2}\}\rho_{13}.
\end{aligned} \tag{25}$$

In the intermediate-field case this term has the form

$$\begin{aligned}
&[\sin^2(\varphi/2)/\tau_x][\tfrac{3}{4}-\tfrac{1}{4}(B_0{}^2-A_0{}^2)\\
&\quad-\tfrac{3}{8}A_0{}^2-\tfrac{1}{4}A_0{}^2B_0{}^2-\tfrac{1}{8}A_0{}^2(B_0{}^2-A_0{}^2)]\rho_{13},
\end{aligned} \tag{26}$$

where the term in brackets has a value less than the high-field result of $\frac{1}{2}$ when both A_0 and B_0 are nonzero.

Writing the correction as $\alpha(X)2I/(2I+1)$, where the $2I/(2I+1)$ is present even in high field, the

effective spin-spin relaxation rate is given by

$$(\tau_2')^{-1} = T_1^{-1} + \alpha[2I/(2I+1)]T_x^{-1}. \qquad (27)$$

Because in intermediate field $\alpha < 1$ ($\alpha = 1$ in the limit of high field), it is seen from Eq. (27) that the spin-exchange rate T_x^{-1} is less effective in broadening the resonance linewidth than in high field. Therefore, the spin-exchange cross section which is computed from $(\tau_2')^{-1}$ must be increased by a factor $(1/\alpha)$.

In order to determine the intermediate-field correction factor α for the transitions which were studied in the alkalis, it is necessary to compute the term analogous to Eq. (26).

The general form of α for the two transitions studied in Rb^{87} and Cs^{133} is given in Table I. In Table II the numerical value of α at the resonant magnetic field is given for these transitions, and in Fig. 3 is a plot of $\alpha(X)$ versus X for Rb^{87} and Cs^{133}.

There are two assumptions implicit in this calculation. First, that only the off-diagonal matrix elements corresponding to resonantly coupled states need be considered, and second, that the spin system remain close to thermal equilibrium $[\rho_{ii} \approx 1/2(2I+1)]$. Both of these approximations are valid to a very high degree for the measurements reported here; that is, the lines were well resolved and studied at power levels well below saturation.

V. DENSITY MEASUREMENT

The linewidth and density measurements were made with a conventional X-band EPR spectrometer. A block diagram of the spectrometer is given in Fig. 4.

The double microwave cavity was rectangular and operated in the TE_{104} mode. Two sets of modulation coils provided field modulation separately to each half of the cavity. A field modulation frequency of 100 kHz was used along with a 10-kHz

TABLE I. General form of the intermediate-field correction factor α for Rb^{87} and Cs^{133}

	Observed transition and basis states	$\alpha(x)$
Rb^{87}	$\lvert F=2, M=-2\rangle = \lvert M_I=-\frac{3}{2}, M_S=-\frac{1}{2}\rangle$	$\alpha(x) = [\frac{3}{4} - \frac{1}{4}(B_{-1}^2 - A_{-1}^2) - \frac{1}{8}A_{-1}^2 B_{-1}^2$
($I=\frac{3}{2}$) to	$\lvert F=2, M=-1\rangle = A_{-1}\lvert M_I=-\frac{3}{2}, M_S=\frac{1}{2}\rangle$	$-\frac{1}{16}A_{-1}^2(B_{-1}^2 - A_{-1}^2) - \frac{3}{16}A_{-1}^2]$
	$+B_{-1}\lvert M_I=-\frac{1}{2}, M_S=-\frac{1}{2}\rangle$	
	$\lvert F=2, M=0\rangle = A_0\lvert M_I=-\frac{1}{2}, M_S=\frac{1}{2}\rangle$	$\alpha(x) = [\frac{3}{4} - \frac{1}{4}A_0^2(B_{-1}^2 - A_{-1}^2) + \frac{1}{4}B_0^2(B_{-1}^2 - A_{-1}^2)$
	$+B_0\lvert M_I=\frac{1}{2}, M_S=-\frac{1}{2}\rangle$	$-\frac{1}{8}A_{-1}^2A_0^2B_0^2 - \frac{1}{8}A_{-1}^2A_0^2B_{-1}^2 - \frac{1}{16}A_{-1}^2A_0^2(A_0^2 - B_0^2)$
to	$\lvert F=1, M=-1\rangle = A_{-1}\lvert M_I=-\frac{1}{2}, M_S=-\frac{1}{2}\rangle$	$+\frac{1}{16}A_{-1}^2A_0^2(B_{-1}^2 - A_{-1}^2) - \frac{1}{8}A_1^2A_0^2]$
	$-B_{-1}\lvert M_I=-\frac{3}{2}, M_S=\frac{1}{2}\rangle$	
Cs^{133}	$\lvert F=4, M=-4\rangle = \lvert M_I=-\frac{7}{2}, M_S=-\frac{1}{2}\rangle$	$\alpha(x) = [\frac{3}{4} - \frac{1}{4}(B_{-3}^2 - A_{-3}^2) + \frac{1}{32}A_{-3}^2(B_{-3}^2 - A_{-3}^2)$
($I=\frac{7}{2}$) to	$\lvert F=4, M=-3\rangle = A_{-3}\lvert M_I=-\frac{7}{2}, M_S=\frac{1}{2}\rangle$	$-\frac{1}{16}A_{-3}^2B_{-3}^2 - \frac{3}{32}A_{-3}^2]$
	$+B_{-3}\lvert M_I=-\frac{5}{2}, M_S=-\frac{1}{2}\rangle$	
	$\lvert F=3, M=-3\rangle = A_{-3}\lvert M_I=-\frac{5}{2}, M_S=-\frac{1}{2}\rangle$	$\alpha(x) = [\frac{3}{4} - \frac{1}{4}A_{-2}^2(B_{-3}^2 - A_{-3}^2) + \frac{1}{4}B_{-2}^2(B_{-3}^2 - A_{-3}^2)$
	$-B_{-3}\lvert M_I=-\frac{7}{2}, M_S=\frac{1}{2}\rangle$	$-\frac{1}{32}A_{-3}^2A_{-2}^2(A_{-2}^2 - B_{-2}^2) - \frac{1}{16}A_{-3}^2A_{-2}^2B_{-2}^2 - \frac{1}{16}A_{-3}^2A_{-2}^2B_{-3}^2$
to	$\lvert F=4, M=-2\rangle = A_{-2}\lvert M_I=-\frac{5}{2}, M_S=\frac{1}{2}\rangle$	$-\frac{1}{32}A_{-3}^2A_{-2}^2(A_{-3}^2 - B_{-3}^2) - \frac{1}{16}A_3^2A_2^2]$
	$+B_{-2}\lvert M_I=-\frac{3}{2}, M_S=-\frac{1}{2}\rangle$	

TABLE II. Numerical values of α for the two transitions which were studied in Rb^{87} and Cs^{133}.

	Transition	Magnetic field B_0 (G)	X	α
Rb^{87}	$\lvert F=2, M=-2\rangle$ to $\lvert F=2, M=-1\rangle$	4795	1.964	0.977
	$\lvert F=2, M=0\rangle$ to $\lvert F=1, M=-1\rangle$	2917	1.195	0.920
Cs^{133}	$\lvert F=4, M=-4\rangle$ to $\lvert F=4, M=-3\rangle$	5804	1.767	0.965
	$\lvert F=3, M=-3\rangle$ to $\lvert F=4, M=-2\rangle$	4125	1.256	0.875

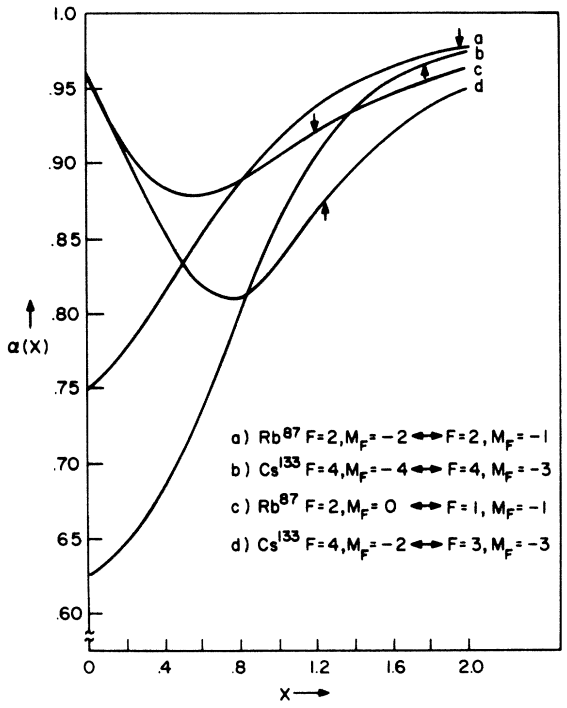

FIG. 3. Intermediate-field correction factor α versus $X=[2g_s\mu_0B_0/(2I+1)A]$.

automatic frequency control. There was no measurable cross talk between the coils. The 100-kHz field modulation amplitude was always a small enough fraction of the resonance linewidth that the phase detected signal was an accurate representation of the first derivative of the Lorentzian absorption line shape.

The alkali sample bulb was held in a Dewar in the back half of the cavity. The bulb was inserted from the top, and the annular space between the bulb and the open top of the Dewar was plugged with asbestos tape. The heated air was then blown in through the side of the Dewar, down past the bulb, and out the bottom.

The front half of the cavity held the copper sulfate standard. Cooling air was blown into the bottom of the front Dewar, past the copper sulfate crystal, and out the top.

With the quartz Dewar in place and a sleeve of precision bore quartz tubing inside each Dewar to simulate operating conditions, the cavity oscillated at 9200 MHz, with a loaded Q of about 3000.

The average rate of energy absorption by a paramagnetic sample is given by Eq. (22)

$$P(\omega)=2\omega\chi''(\omega)H_1^2,$$

where H_1 is the amplitude of the microwave field, ω is the resonance frequency, and $\chi''(\omega)$ is the imaginary part of the complex rf magnetic susceptibility.

The question of how to relate the energy absorbed by the paramagnetic sample to the signal observed with an EPR spectrometer is a bit complicated. It has been discussed in general in the literature,[16] and a detailed application to an experiment like the present one has been discussed by Moos.[8] It is found that using small amplitude field modulation and phase detection, the signal is proportional to the following quantities:

$$(P^C)^{1/2},\quad \eta,\quad \frac{\partial\chi''}{\partial H},\quad \text{and}\quad (H_m)_{\text{eff}},$$

where (a) $(P^C)^{1/2}$ is the square root of the power incident upon the cavity, (b) η is the filling factor,

$$\eta=\int_{\text{sample}} H_1^2\,dV_{\text{sample}}\Big/\int_{\text{cavity}} H_1^2\,dV_{\text{cavity}},$$

(c) $(H_m)_{\text{eff}}$ is the "effective" modulation field, given by

$$(H_m)_{\text{eff}}=\int_s H_m H_1^2\,dV_s\Big/\int_s H_1^2\,dV_s,$$

and (d) $\partial\chi''/\partial H$ is the rate of change of the imaginary part of the rf susceptibility with external field.

Using the Lorentzian form of $\chi''(\omega)$ given in Sec. II, we have that the maxima of the first derivative signals are given by

$$(S)_{\max}=\text{const}\times\frac{(H_m)_{\text{eff}}N\mu_0^2|\langle i|\sigma_x|j\rangle^2\omega_{ij}}{2(2I+1)T(\Delta H)^2(\partial\omega/\partial H)},\qquad(28)$$

where N is the number density, ω_{ij} is the resonance frequency, I is the nuclear spin, T is the temperature, ΔH is the separation in Gauss between peaks of the first derivative signal, and $\partial\omega/\partial H$ is the rate of change of the resonance fre-

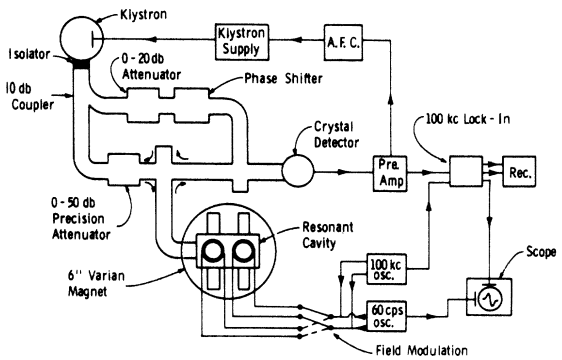

FIG. 4. Block diagram of EPR spectrometer.

quency with field at the resonant field. The linewidth for the first derivative of the Lorentzian is given by

$$\Delta H = \frac{2}{\sqrt{3}} \left(\frac{\partial \omega}{\partial H} \right)^{-1} \frac{2I\alpha}{2I+1} \frac{1}{T_x}$$

and the constant includes factors like spectrometer gain settings.

The principle of making an absolute determination of density using an EPR spectrometer is to take a ratio of the area under the absorption spectrum for the alkali, where N is unknown, to this area for a standard, for which N is known.

The standard in the present experiment is copper sulfate, where N is determined by weighing the individual crystal with a microbalance.

The X-band EPR spectrum of copper sulfate has been studied,[17,18] and the anisotropic g values have been determined. By proper orientation one can arrange to have the "g value" along the dc field equal to 2.09, and the "g value" normal to the dc field (parallel to the oscillating magnetic field) equal to 2.25. The $g = 2.25$ measures the component of the Cu^{++} ions magnetic moment which couples to the oscillating magnetic field producing the transition. With this orientation, the linewidth was about 30 G, and the line shape was Lorentzian out to about 10 linewidths, as shown in Fig. 5.

A comparison of the alkali line shape to a Lorentzian is shown in Fig. 6.

In order to obtain a specific expression for the alkali density, it is necessary to calculate $(H_M)_{\text{eff}}$ for both the alkali and the copper sulfate crystal.

Since the copper sulfate crystal is small compared to the dimensions of the cavity, the variation of $H_M H_1^2$ and H_1^2 over the crystal was negligible. However, the alkali was a distributed sample so it was necessary to probe the distribution of $H_M H_1^2$ and H_1^2 over the length of the active volume of the alkali. This was done with a small piece of diphenylpicrylhydrazl (DPPH). As shown in Fig. 7 the $H_M H_1^2$ points were a very good fit to $\cos^3(2\pi x/\lambda)$, with $\lambda/2 = 2.4$ cm, and as shown in Fig. 8 the H_1^2 fit $\cos^2(2\pi x/\lambda)$, with $\lambda/2 = 2.4$ cm.

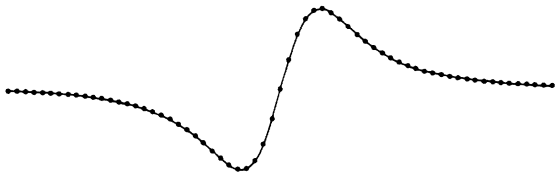

FIG. 5. Comparison of a $CuSO_4$ line shape to a Lorentzian.

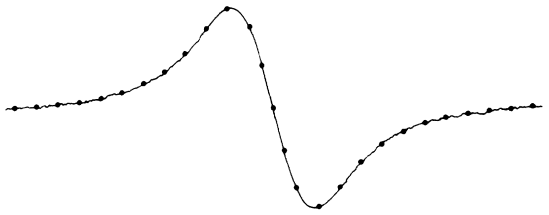

FIG. 6. Comparison of an alkali line shape to a Lorentzian.

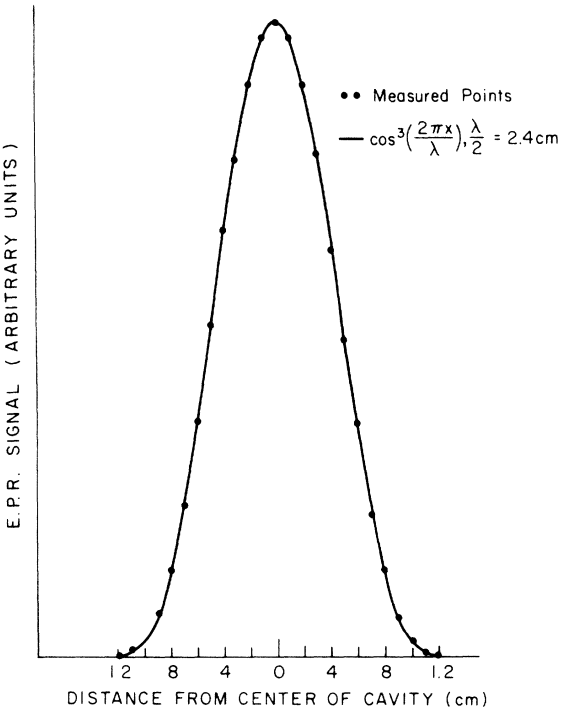

FIG. 7. Variation of the EPR signal, which is proportional to $H_M H_1^2$, over the length of the alkali sample bulb.

Using these distributions one finds for the filling factor

$$\frac{N_{\text{alkali}}}{N_{CuSO_4}} = \frac{\frac{1}{2} \text{ volume of alkali}}{\text{volume of } CuSO_4},$$

and for the effective modulation fields

$$\frac{[(H_M)_{\text{eff}}]_{\text{alk}}}{[(H_M)_{\text{eff}}]_{CuSO_4}} = 0.849$$

These can be combined, using Eq. (28), to give an expression for the alkali density

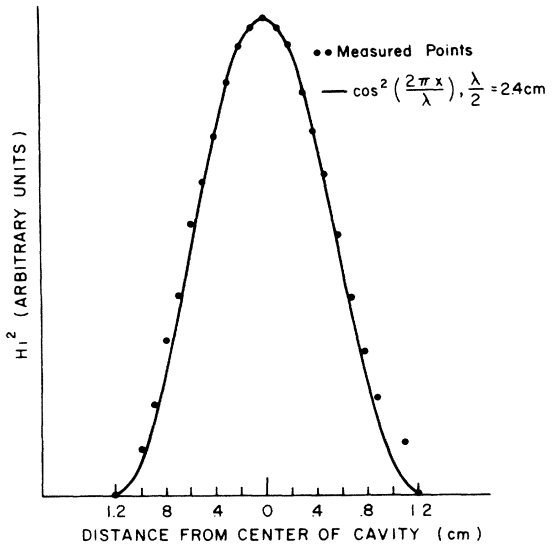

FIG. 8. Variation of the microwave field intensity H_1^2, over the length of the alkali sample bulb.

$$N_{\text{alkali}} = \text{const}\,(2I+1)\frac{S_{\text{alk}}}{S_{\text{CuSO}_4}} \times \frac{(\partial\omega/\partial H)_{\text{alk}}}{|\langle i|\sigma_x|j\rangle|^2_{\text{alk}}} \frac{(\Delta H)^2_{\text{alk}}}{(\Delta H)^2_{\text{CuSO}_4}} \frac{T_{\text{alk}}}{T_{\text{CuSO}_4}},$$

where S is the peak amplitude of the first derivative signal, and the constant takes account of all the numerical factors which enter Eq. (28).

Table III lists the values of $\partial\omega/\partial H$ as calculated from the Breit-Rabi[13] formula, and the electron-spin transition matrix elements as calculated from the eigenfunctions of the Breit-Rabi eigenvalues.

VI. EXPERIMENTAL PROCEDURE

This section will describe the preparation of the alkali sample bulbs and the copper sulfate standard, calibration of the magnetic field sweep, and the data taking procedure.

A. Sample Preparation

This section is divided into two parts because two different kinds of sample bulbs were used. Precision bore quartz tubing was used for Cs^{133}, Rb^{87}, Rb^{85}, and K^{39}. At the requisite temperature of about 700°K for Na^{23}, the vapor reacts so quickly with the quartz that it is impossible to obtain any data for sodium with quartz bulbs. A special container constructed from a sodium vapor resistant aluminum oxide was used for Na^{23}.

1. Quartz Sample Bulbs

The quartz sample bulbs were made from Amersil precision bore quartz tubing, as shown in Fig. 9. The inside diameter was 4 mm and the outside diameter ranged from 6.10 to 6.25 mm. A four-inch length of this tubing was attached to an L-shaped section of quartz capillary tubing. A one-half inch diameter reservoir on the end of this capillary contained some cool alkali which served to getter impurity gases which might be released during a run.

To fill the quartz bulbs with Cs^{133}, Rb^{87}, and Rb^{85}, the appropriate alkali chloride was crushed with calcium hydride and the mixture was placed in a pyrex distilling manifold. After evacuation, gentle heating with a torch drove off hydrogen gas. Further heating caused the alkali to condense in the manifold, from which it was driven into the quartz bulb.

The CsCl was reagent grade with a stated purity of 99.95%. An optical spectroscope was set up in our laboratory to check the identity and purity of the materials used in this experiment. The spectroscope was found to be able to detect about 2% alkali impurity, and to this accuracy the CsCl was found to contain only cesium.

Isotopically pure RbCl was purchased from Oak

TABLE III. Rate of change of resonance frequencies with respect to external magnetic field and transition matrix elements at the resonant magnetic fields.

Alkali	Transition	Field (G)	$\partial\omega/\partial H$ (10^6 sec^{-1}/G)	$\langle F\|\sigma_x\|I\rangle$
Cs^{133}	$M_F=-4 \rightarrow M_F=-3$	5804	16.2	0.949
	$M_F=-3 \rightarrow M_F-2$	4125	11.3	0.816
Rb^{87}	$M_F=-2 \rightarrow M_F=-1$	4795	16.4	0.964
	$M_F=-1 \rightarrow M_F=0$	2917	12.3	0.845
Rb^{85}	$M_F=-3 \rightarrow M_F-2$	4110	17.2	0.993
K^{39}	$M_F=-2 \rightarrow M_F=-1$	3375	17.6	1.00
Na^{23}	$M_F=-1 \rightarrow M_F=0$	3370	17.6	1.00

Ridge National Laboratory. The stated purity for Rb^{85} was 99.54%, and for Rb^{87} it was 99.10%.

The K^{39} was purchased as the pure metal in 2-g glass ampules. The top of one of these ampules was broken off and it was dropped into the distilling manifold, the manifold then being quickly sealed and evacuated. Heating the glass ampule caused K^{39} to condense in the manifold from which it was driven into the quartz sample bulb. The stated purity of the K^{39} was 99.9%, and our spectrographic analysis revealed no detectable alkali impurities.

When the desired amount of alkali had been driven into the bulb, it was sealed and removed from the vacuum system. The pressure at seal-off was always 10^{-5} mm Hg or lower.

2. *Coram Sample Bulb*

Coram[19] is a sodium vapor resistant fused aluminum oxide which was developed by the Corning Glass Works. The outside diameter of the Coram tube was 0.200 in. and the inside diameter was 0.136 in. A $\frac{1}{8}$-in.-diam niobium tube was sealed to the Coram by Corning with a special frit, as shown in Fig. 10.

The niobium tube is quite ductile initially, but becomes brittle upon heating in air. This prevented distilling the sodium into the Coram bulb. It was decided to fill the bulb with small chips of pure sodium metal under a nitrogen atmosphere. The niobium tube was then attached to a stopcock copper-to-glass seal assembly by means of a Swage-Lok vacuum connector.

Without admitting any air this assembly was attached to the vacuum system, after which the stopcock was opened in order to evacuate the Coram bulb. When the system had reached a pressure of 5×10^{-5} mm Hg or lower, the assembly was removed from the vacuum system by melting the Pyrex between the stopcock and the copper-to-glass seal.

To prevent the alkali from migrating from the Coram bulb to the Swage-Lok during a run, the still ductile niobium was pinched in two or three places by a home-made vacuum pinch-off tool. The pinch was enough to cause some plastic flow of the niobium but not enough to sever it completely.

A spectroscopic analysis revealed no alkali impurities in the Na^{23}.

B. Standard Preparation

The standard preparation amounts to weighing out a few $CuSO_4$-$5H_2O$ crystals, gluing them onto a thin pyrex filament with Duco cement, and then comparing the signals of the crystals against their weights to insure internal consistency.

The crystals were weighed on a Cahn Electrobalance to an accuracy of a few micrograms out of about 1.5 mg, with an internal consistency between weights and EPR signal strength of about 1.5%. This scatter reflects the combined error of weighing and misorientation of the crystal.

The center of the pyrex filament was hollow with the end sealed. A small crystal of BDPA[20] was dropped into the top and rested just above the copper sulfate crystal, but was out of contact with the Duco cement because it was found that Duco dissolved the BDPA.

The BDPA was used to measure the microwave field intensity in connection with the T_1 measurements, which are discussed in detail in the Appendix.

1. *Data Taking Procedure*

This section will describe the step-by-step procedure used to acquire the data.

Before making a run the Varian 6-in. magnet was allowed to warm up for at least 3 h. With the alkali bulb in place in the back cavity, the copper sulfate standard was oriented in the front cavity. A length of the same precision bore quartz used in the alkali bulb was placed in the front cavity to ensure that the standard had the same microwave field intensity as the alkali. While still at room temperature two or three traces of the copper

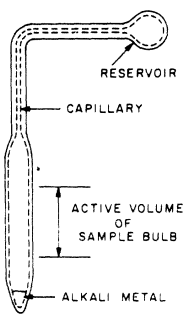

FIG. 9. Quartz sample bulb used to study Cs^{133}, Rb^{87}, Rb^{85}, and K^{39}.

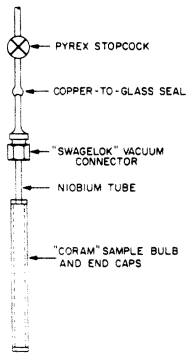

FIG. 10. Coram sample bulb used to study Na^{23}.

sulfate and the BDPA were taken. The linewidths used in density and saturation calculations were taken from these traces.

After this the air was turned on and the heater current adjusted to give the desired alkali temperature. When the temperature had stabilized, at least four traces of the alkali resonance were obtained. Care was taken to avoid either power or modulation broadening. For points where T_1 was to be determined, the alkali signal was then saturated and another trace was run.

The 100-kc/sec field modulation was then switched to the front cavity in order to obtain a trace of the copper sulfate standard. The field modulation and microwave attenuator settings were the same for the alkali and the copper sulfate. This required a change in the phase detector gain setting, but the linearity of this had been checked. For points where T_1 was to be determined, an unsaturated and saturated trace for BDPA was also taken.

At this point the spectrometer was adjusted to the initial settings and two more alkali traces were taken. Any change in conditions during the 10 or 15 min required to take the above data would be reflected by a difference in the alkali signal from beginning to end. If the alkali signals were the same from start to finish, the power to the heater was increased and the above procedure was repeated for another data point. A typical run consisted of six or seven such data points.

All spectrometer settings relevant to data interpretation were written on the chart paper, and the settings were checked repeatedly during a run to avoid errors.

VII. ANALYSIS OF EXPERIMENTAL RESULTS

This experiment measures a resonance linewidth and the corresponding density for a number of different densities. A plot of (ΔH) versus density (N) gives a straight line whose slope is proportional to the cross section for spin exchange, as shown in Figs. 11–15.

In order to obtain a cross section it is necessary to rewrite the general relation from kinetic theory in terms of experimentally determined quantities.

From the Introduction

$$1/T_x = N\langle V\rangle_{\text{rel}}\sigma_x, \tag{29}$$

where $\langle V\rangle_{\text{rel}} = 2^{1/2}(8kT/\pi m)^{1/2}$.

$$\sigma_x = \frac{\sqrt{3}}{2}\,\frac{2I+1}{\alpha(2I)}\,\frac{(\partial\omega/\partial H)}{\langle V\rangle_{\text{rel}}}\left(\frac{\Delta H}{N}\right).$$

For a Lorentzian line the separation, in Gauss, between the peaks of the first derivative signal is

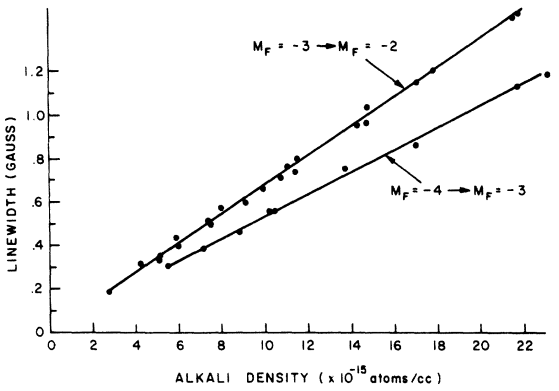

FIG. 11. Linewidth versus density for the two transitions studied in Cs^{133}.

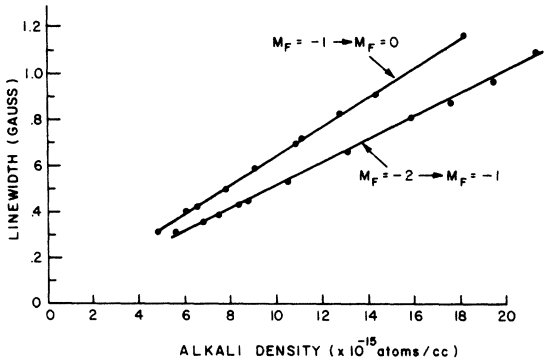

FIG. 12. Linewidth versus density for the two transitions studied in Rb^{87}.

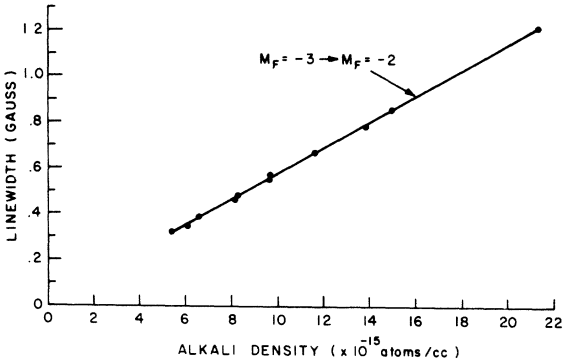

FIG. 13. Linewidth versus density for the transition studied in Rb^{85}.

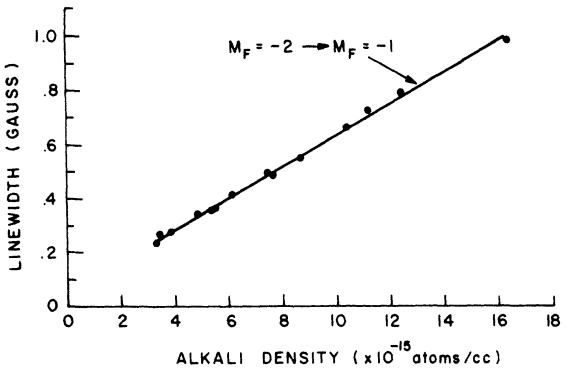

FIG. 14. Linewidth versus density for the transition studied in K^{39}.

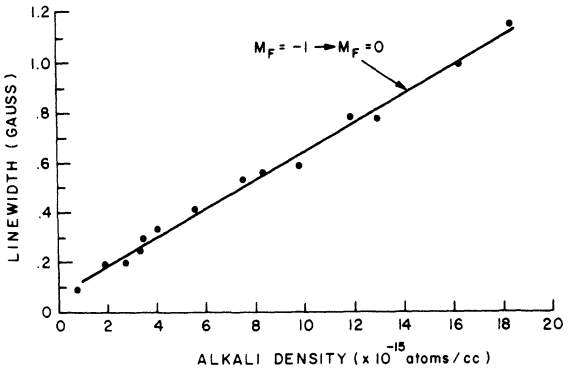

FIG. 15. Linewidth versus density for the transition studied in Na^{23}.

given by

$$\Delta H = \frac{2}{\sqrt{3}}\left(\frac{\partial\omega}{\partial H}\right)^{-1}\frac{\alpha 2I}{2I+1}\frac{1}{T_x}.$$

This gives from Eq. (29)

In order to eliminate any contributions from density-independent broadening mechanisms, we can substitute for $\Delta H/N$ the slope of the line, which is written here as $\delta(\Delta H)/\delta N$.

This gives

$$\sigma_x = \frac{\sqrt{3}}{2}\frac{(2I+1)}{2I\alpha}\frac{(\partial\omega/\partial H)}{\langle V\rangle_{\text{rel}}}\frac{\delta(\Delta H)}{\delta N}.$$

The intermediate-field correction α for Cs^{133} and Rb^{87} was discussed in Sec. II.

Table IV lists the spin-exchange cross sections for all the alkali transitions which were studied and, in addition, the theoretical cross sections of Dalgarno and Rudge[21] recomputed by us at the experimental temperatures. A comparison of the experimental and theoretical numbers is consistent with the estimate of Dalgarno and Rudge that the theoretical cross sections are less than 30% below the true values.

VIII. ERROR ANALYSIS

This section will discuss the sources of error which affect the accuracy of the spin-exchange cross sections. From an operational point of view the errors to be considered are those which affect the slope of the linewidth versus density line. The error in measuring the linewidth is easily estimated and does not contribute greatly to the over-

TABLE IV. Spin-exchange cross sections.

Element	Transition	Temperature (°K)	Experimental (10^{-14} cm^2)	Theoretical[a] (10^{-14} cm^2)
Cs^{133}	$M_F=-4 \rightarrow M_F=-3$	500	$2.06^{+0.17}_{-0.27}$	1.90
	$M_F=-3 \rightarrow M_F=-2$	500	$2.05^{+0.17}_{-0.27}$	
Rb^{87}	$M_F=-2 \rightarrow M_F=-1$	550	$1.84^{+0.15}_{-0.24}$	1.65
	$M_F=-1 \rightarrow M_F=0$	550	$1.86^{+0.15}_{-0.24}$	
Rb^{85}	$M_F=-3 \rightarrow M_F=-2$	550	$1.92^{+0.15}_{-0.25}$	
K^{39}	$M_F=-2 \rightarrow M_F=-1$	600	$1.45^{+0.12}_{-0.19}$	1.45
Na^{23}	$M_F=-1 \rightarrow M_F=0$	700	$1.03^{+0.09}_{-0.14}$	1.05

[a]Reference 21.

all error in the experiment. The density measurement is by far the largest source of error. As shown in Sec. III, there are 15 calculated or measured quantities which enter the expression for density. In addition, the expression itself rests upon the assumption that the alkali and copper sulfate lines are Lorentzian.

The various sources of error are considered below. In each case the maximum error in percent is estimated. A summary of the errors is given at the end.

A. T_1 Correction

It is important to convince oneself that the only density-dependent contribution to ΔH is spin exchange. This is not strictly true because any collision which relaxes the spin will give a density-dependent contribution to ΔH. In fact, the entire experiment rests upon the assumption that spin exchange constitutes so large a contribution to ΔH that the combined effect of all other density-dependent broadening mechanisms is either negligible or can be determined to the necessary precision.

The Appendix considers the question of how to determine experimentally the presence of density-dependent broadening mechanisms in addition to spin exchange. A measurement of the thermal relaxation rate $(T_1)^{-1}$ reflects the collective effect of mechanisms which contribute not only to the linewidth (a τ_2 process) but also to the energy relaxation of the spin system (a τ_1 process).

It is still possible for density-dependent processes to contribute to τ_2 but not τ_1. Such processes would not be included in the T_1 measurement reported in the Appendix.

The conclusion reached in the Appendix is that the T_1 correction to the measured linewidth is negligible for Rb^{87}, Rb^{85}, K^{39}, and Na^{23}.

As is discussed in the Appendix, there persists a small, but not negligible, contribution to the linewidth from T_1 processes for both of the transitions studied in Cs^{133}. There is some evidence to indicate that this correction is too large, but in the absence of a conclusive argument to ignore it, a -3% error was allowed for the Cs^{133} data.

B. Field Sweep Calibration

The internal consistency of the sweep calibration was $\pm 1\%$. A check of the sweep rate after three months gave the same sweep rate to within $\pm 1\%$. An estimate of the extreme error is $\pm 2\%$.

C. g Values for $CuSO_4$-$5H_2O$

When the freshly weighed $CuSO_4$-$5H_2O$ crystals were glued to the Pyrex filament, they were attached in such a way that the g value along the dc magnetic field could be adjusted to 2.09 by rotating the filament. This 2.09 is felt to be known to $\pm \frac{1}{2}\%$. The crystals were attached such that the g value along the microwave field varied from 2.24 to 2.26, so we can say the matrix element M_{ij} is known to $\pm \frac{1}{2}\%$. The combined error of weighing and misorientation is reflected by the consistency of $\pm 1.5\%$ between $\Delta S(\Delta H)^2$ and weights for the four crystals which were compared prior to taking the data reported in Sec. V.

The combined error in the density caused by uncertainties in the g values of copper sulfate is estimated to be $\pm 4\%$.

D. Ratio of Signals from Front and Back Cavity

If it were to occur that the signal from one part of the cavity were different from the signal from the other part, due presumably to some asymmetry in the cavity, then one would have to take this difference into account when comparing signals.

Care was taken to ensure that the environments were similar in both halves of the double cavity. However, a comparison of signals from front to back showed a larger signal in front by a factor of about 1.33.

A measurement of the modulation field amplitudes in front and back for a wide range of gain settings gave ratios between 1.30 and 1.35. This seems to verify that the difference is due to different modulation field amplitudes. An estimate of the extreme error of this correction is $\pm 4\%$.

E. Variation of Quartz Tubing

The maximum variation of the outside diameters of the precision bore quartz tubing was 0.006. The K^{39} data were taken with two different bulbs. There was no systematic difference which could be attributed to differences in the quartz tubing. An estimate of the error due to differences in the o.d. of the quartz tubing is $\pm 1\%$.

E. Films

After an hour or two at operating temperature the quartz bulb is observed to develop a brown color on the inside. Moos[8] concluded that the effect of this film was only to reduce the Q of the cavity. This is consistent with the observation of the Rb^{85} data. Runs were made with a new bulb and with the same bulb after the dark film had developed. There was a reduction of the Q of the cavity, but the data showed no systematic shift. It is concluded that these films cause no error in the measurement of the spin-exchange cross section.

G. Determination of $(H_m)_{\text{eff}}$

The definition of $(H_m)_{\text{eff}}$ is

$$(H_m)_{\text{eff}} = \int H_m H_1^2 dV_s / \int H_1^2 dV_s .$$

The variation of $H_m H_1^2$ and H_1^2 over the volume of the sample must be determined in order to evaluate these integrals.

Plots of the variation of $H_m H_1^2$ and H_1^2, Figs. 7 and 8, in the vertical plane agreed quite well with $\cos^3(2\pi x/\lambda)$ and $\cos^2(2\pi x/\lambda)$, respectively, with $\lambda/2 = 2.4$ cm. In the absence of any fringing fields in the chimneys where the Dewars fit into the cavities, the half-wavelength would be 2.29 cm. The experimentally determined $\lambda/2 = 2.4$ cm indicates a small amount of fringing.

The variation of $H_m H_1^2$ across a diameter of the bulb was probed with a piece of BDPA attached to the end of a thin pyrex filament. As the BDPA was moved from one side of the inside of the bulb to the other, the EPR signal, as viewed on an oscilloscope, did not change amplitude. Therefore this variation is ignored. The error in determining $(H_m)_{\text{eff}}$ is estimated to be $\pm 2\%$.

H. Determination of Sample Volume

The active volume of the alkali sample is determined by the inside diameter of the precision bore quartz tubing (or the Coram), and the distance over which $H_m H_1^2$ is nonzero. Because of the good fit of $H_m H_1^2$ to $\cos^3(2\pi x/\lambda)$, where $\lambda/2 = 2.4$ cm, and the fact that no reversal of the signal appeared beyond $x = \pm 1.2$ cm, it is assumed that the active volume of the sample is known to within $\pm 2\%$.

I. Line Shapes

The line shape of the alkali and the copper sulfate must be considered.

1. *Alkali*

The alkali resonance line is expected theoretically to be Lorentzian. The comparison of theoretical and experimental data given in Fig. 6 justifies this assumption.

2. *Copper Sulfate*

The assumption of a Lorentzian for copper sulfate is not as clearly justified as for the alkali. However, the theoretical and experimental comparison given in Fig. 6 indicates that this is a very good assumption. The maximum possible error in the cross section from assuming this line is Lorentzian is estimated to be -5%.

J. Temperature Measurements

The temperatures of the alkali and the copper sulfate were measured with copper-constantan thermocouples. The calibration of the thermocouples was checked in boiling water.

1. *Copper Sulfate*

In order to prevent the $CuSO_4$-$5H_2O$ crystals from reaching 40°C and thereby losing water of hydration, cooling air was blown through the front Dewar. The temperature was measured and was assumed known to $\pm \frac{1}{2}\%$.

2. *Alkali*

In the initial stages of the experiment, the Dewar which held the alkali was identical to the one in the front half of the cavity. This required the alkali bulb to be inserted from the top and the hot air to be blown in from the bottom. This design favored a temperature gradient along the bulb from the bottom to the top of the bulb. With this arrangement the alkali melt tended to migrate from the bottom to the top of the bulb. While this migration was going on there were two melts at different temperatures supplying the vapor.

In an effort to reduce these gradients, a quartz Dewar was constructed which permitted the hot air to be blown in from the top and the sample bulb to be inserted from the top. With this arrangement, any temperature gradient which might exist would favor the alkali melt remaining at the bottom of the bulb.

A sample bulb was constructed which could be evacuated and which contained three copper-constantan thermocouples. The temperatures of these thermocouples were compared with that of another thermocouple which was placed in the airstream at the position it occupied during the experiment. At 600°K the external thermocouple agreed with the average of the three internal thermocouples to within $1\frac{1}{2}\%$. The gradient at 600°K was approximately 1%. The error in determining the alkali temperature is estimated to be $\pm 2\%$.

K. Linewidth Determination

The linewidth as used here refers to the width in Gauss between peaks of the first derivative signal. For a signal having observable noise, the position of the peak can be difficult to locate and would contribute a sizable error to the cross sections.

However, because of the finite slope, it was much easier to locate the point in the wings where the signal had fallen to half its peak value. So-

lution of the equation for a Lorentzian line shows that the separation of these points is 2.56 times the linewidth as defined above. The error in determining the linewidth using this method is estimated to be ±3%.

L. Electronic Errors

To account for possible errors in amplifier and recorder gain settings and linearity an error of ±3% is included.

M. Summary

The estimated maximum errors are summarized in Table V. It is not possible to say with certainty how these will collectively affect the cross section. If one just adds the errors, the maximum error is $^{+22\%}_{-27\%}$.

If it is assumed that the errors which have a ± sign are random, then one can take the square root of the sum of the squares of these terms. Including the −5% line-shape error this gives $^{+8\%}_{-13\%}$.

In order to make an estimate of the accuracy of the relative cross sections, we can take the square root of the sum of the squares of those terms which could change from one run to the next. This gives ±6½% for the relative cross sections.

IX. SUMMARY

This paper has reported an electron-spin-resonance study of the magnetic hyperfine transitions in the ground state of the alkalis Cs^{133}, Rb^{87}, Rb^{85}, K^{39}, and Na^{23}. The spin-exchange cross sections were determined through the broadening of the absorption spectrum by spin-exchange collisions.

This work has contributed to the expanding spin-exchange data in the following three general areas:

(1) The spin-exchange cross section for Na^{23} of

$$\sigma_x = 1.03^{+0.09}_{-0.14} \times 10^{-14}\,\mathrm{cm}^2$$

is the first determination of this number to an accuracy better than a factor of 3.

(2) Measurements on two different transitions of Cs^{133} and Rb^{87} have demonstrated the importance of the intermediate-field correction.

(3) The measurement of the self spin-exchange cross sections for all the alkalis by the same apparatus affords a more accurate determination of the relative cross sections than has been known. These are given in Table VI.

TABLE V. Estimated errors.

Field sweep calibration	± 2%
g values for $CuSO_4$-$5H_2O$	± 4%
Ratio of signals in front and back	± 4%
Variation of quartz tubing	± 1%
$(H_m)_{\mathrm{eff}}$	± 2%
Alkali volume	± 2%
$CuSO_4$-$5H_2O$ line shape	−5%
Temperature measurement	± 2%
Linewidth determination	± 3%
Electronic	± 3%
T_1 correction for Cs^{133}	−3%

APPENDIX

In order to account explicitly for an energy relaxation mechanism, we must add an additional term to the equation of motion for the "average" density matrix which takes the "average" matrix toward thermal equilibrium. This gives

$$\frac{d\rho}{dt} = -\frac{i}{\hbar}[\mathcal{H},\rho] - \frac{1}{\tau_c}(\rho-\rho_c) - \frac{1}{T_1}(\rho-\rho_0).$$

As shown in Sec. II the steady-state solutions of this equation lead to the following effective spin-spin and spin-lattice relaxation rates:

$$\frac{1}{\tau_2} = \frac{1}{T_1} + \left(\frac{2I}{2I+1}\right)\frac{1}{T_x}, \qquad \frac{1}{\tau_1} = \frac{1}{T_1} + \frac{1}{T_1/2I + [(2I+1)/2I]\,T_x}. \tag{30}$$

The method used to study the τ_1 rate was to saturate the EPR signal. Providing that the functional dependence of $\chi''(\omega)$ upon H_1^2 and τ_1 is known, it is possible to determine τ_1 from the saturation data.

It was assumed that the saturation term enters the rf susceptibility for the multilevel system in the same way as for a two-level system. Thus one has for $\chi''(\omega)$

TABLE VI. Relative spin-exchange cross sections.

$\sigma_{Cs^{133}}/\sigma_{Na^{23}}$	2.00 ± 0.18
$\sigma_{Rb^{87}}/\sigma_{Na^{23}}$	1.80 ± 0.16
$\sigma_{Rb^{85}}/\sigma_{Na^{23}}$	1.86 ± 0.17
$\sigma_{K^{39}}/\sigma_{Na^{23}}$	1.41 ± 0.13

$$\chi''(\omega) = \frac{N\mu_1^2 |\langle i|\sigma_x|j\rangle|^2 \omega_{ij}\tau_2}{2(2I+1)kT[1+(\omega_{ij}-\omega)^2\tau_2^2+\gamma^2 H_1^2\tau_1\tau_2]}.$$

The saturation factor $A=\gamma^2 H_1^2\tau_1\tau_2^2$ can be measured by comparing signal amplitudes with and without saturation. Independent determination of H_1^2 and τ_2 then permits one to solve for τ_1.

τ_2 was determined from the unsaturated linewidth. H_1^2 was measured by saturating the organic free radical $\alpha\gamma$-bisdiphenylene-β-phenyl allyl (BDPA). This material was chosen because it has $\tau_1=\tau_2$ and was saturable under our experimental conditions.

This seemingly simple procedure is complicated by the fact that the microwave field intensity H_1^2 varies over the length of the sample. The greater saturation at the center of the alkali tends to make the top and bottom of the sample contribute proportionally more to the signal than they would normally. One must average over this variation in order to predict the effect of saturation upon the signal.

When this is done one can plot a curve of the ratio of unsaturated to saturated signal amplitude as a function of the saturation factor A.

Knowing τ_1 from saturation and calculating τ_2 from the unsaturated linewidth, one can use Eq. (30) relating τ_1, τ_2, T_1, and T_χ to solve for T_1 and T_χ.

Saturation measurements were carried out for all of the alkalis which were studied. For Na^{23} and K^{39} the maximum contribution of T_1 to the measured linewidth was completely negligible. For Rb^{85} and Rb^{87} the contribution of T_1 was certainly less than $\frac{1}{2}\%$, and because of the inaccuracy of the saturation measurements this contribution was ignored.

The saturation data for Cs^{133} were internally contradictory. The T_1 correction to ΔH resulted in a shift in the ΔH-versus-N line without changing its slope, which would not affect the measured spin-exchange cross section. However, the shift produced a small negative ΔH intercept at zero density, which is clearly impossible.

The assumption that one can characterize a multilevel system by a single saturation factor, particularly a system like Cs^{133} having 16 sublevels which are unequally spaced in intermediate field, is highly suspect and may well be the source of the problem.

In order to encompass the largest contribution of T_1, an allowance of -3% was included. This reflects the largest change in slope of ΔH versus N which could result from the T_1 correction.

---

†Most of this work is taken from the theses of two of the authors (N. W. Ressler and T. E. Stark) submitted in partial fulfillment of the requirements for the Ph. D. at the University of Michigan.

*Work carried out with the partial support of the U. S. Atomic Energy Commission.

‡General Motors Graduate Fellow, 1962–67.

[1]E. M. Purcell and G. B. Field, Astrophys. J. 124, 542 (1956).

[2]J. P. Wittke and R. H. Dicke, Phys. Rev. 103, 620 (1956).

[3]H. G. Dehmelt, Phys. Rev. 109, 381 (1958).

[4]P. L. Bender, Phys. Rev. 136, 2154 (1964).

[5]J. Vanier, Phys. Rev. 168, 129 (1968).

[6]S. B. Crampton, Phys. Rev. 158, 57 (1967). This paper has references to many previous papers on spin-exchange shifts.

[7]H. M. Gibbs and R. J. Hull, Phys. Rev. 153, 132 (1967). This paper reports the most accurate measurement to date of spin-exchange cross sections using optical pumping. The bibliography lists previous theoretical and experimental work in spin exchange.

[8]H. W. Moos and R. H. Sands, Phys. Rev. 135, A591 (1964). The method used in the present work was developed by Moos and Sands.

[9]For additional details see T. E. Stark, Ph. D. thesis, University of Michigan, 1966 (unpublished). Other analyses are given by F. Grossetete, J. Phys. 15, 383 (1964); A. E. Glassgold, Phys. Rev. 132, 2144 (1963); A. E. Glassgold and S. A. Lebedoff, Ann. Phys. (N. Y.) 28, 181 (1964).

[10]A. E. Glassgold, Phys. Rev. 132, 2144 (1963).

[11]T. Y. Wu and T. Ohmura, Quantum Theory of Scattering (Prentice-Hall, Inc., Englewood Cliffs, New Jersey, 1962), p. 235.

[12]R. Karplus and J. Schwinger, Phys. Rev. 73, 1020 (1948).

[13]G. Breit and I. Rabi, Phys. Rev. 38, 2082(L) (1930).

[14]A. Abragam, Principles of Nuclear Magnetism (Oxford University Press, London, England, 1961).

[15]For the case of arbitrary nuclear spin I, the term analogous to $[1-(\rho_{11}+\rho_{33})]$ would be $2I/2I+1$ instead of $\frac{1}{2}$.

[16]J. P. Goldsborough and M. Mandel, Rev. Sci. Instr. 31, 1044 (1960).

[17]D. Polder, Physica 9, 709 (1942).

[18]D. M. S. Bagguley and J. H. E. Griffiths, Proc. Roy. Soc. (London) A201, 366 (1950).

[19]The assistance of the Corning Glass Works in providing the Coram sample bulbs is greatly appreciated.

[20]The crystalline organic free radical α, γ-bisdiphenylene-β-phenyl allyl (BDPA) was chosen for the T_1 measurements because it has the property that $T_1=T_2$, and it can be saturated with our spectrometer. Its linewidth is about $\frac{1}{2}$ G.

[21]A. Dalgarno and M. R. H. Rudge, Proc. Roy. Soc. (London) A286, 519 (1965).